Sasikumar, A., García-Rodríguez, S.M., Arbeláez, J.J., Trias, D. i Costa, J. (2020). On how unsymmetrical laminate designs with tailored ply clusters affect compression after impact strength compared to symmetric baseline. *Composite Structures*, vol. 238, art. núm. 111958. Available online at https://doi.org/10.1016/j.compstruct.2020.111958

On how unsymmetrical laminate designs with tailored ply clusters affect compression after impact strength compared to symmetric baseline

A.Sasikumar[a,*], S.M. García-Rodríguez[a], J.J. Arbeláez[a,b], D.Trias[a,1], J.Costa[a,*]

[a] *AMADE, Polytechnic School, University of Girona, Campus Montilivi s/n, 17073 Girona, Spain*
[b] *Engineering Faculty, Instituto Tecnológico Metropolitano (ITM), C.73, No. 76-354, Medellín, Colombia*

Abstract

Out-of-plane loads induce unsymmetrical damage modes in the laminate thickness direction. Consequently, the authors have recently proposed overcoming the conventional laminate symmetry constraint by designing unsymmetrical laminates with zero coupling responses. While impact damage is able to be tailored with unsymmetrical laminates, comparing them to symmetric laminates and assessing their impact damage tolerances had yet to be addressed. In this paper, we study three unsymmetrical laminates with localized ply clusters positioned at different locations (at the impacted, at the middle and at the non-impacted sides), along with a standard symmetric laminate as a baseline. Using low-velocity impact, X-ray micro-computed tomography and compression after impact (CAI), we compared the impact and post-impact responses to understand the effect local ply clusters and the delamination location have on the CAI strength. Results revealed that the unsymmetrical laminate with the ply clusters in the middle, where the dominant delaminations also occured, improved the CAI strength by a maximum of 10% when compared to the symmetric baseline. Laminates with delaminations at the outer surfaces offered lesser resistance to buckling. While our study demonstrates that symmetric laminates are not the optimal damage tolerant solution for impact load cases, it also evidences the feasibility of unsymmetrical laminates.

Keywords: Delamination, Impact behaviour, Damage tolerance, Unsymmetrical laminates

---

1. Introduction

Low velocity impact loads continue to be one of the load case threats that aircraft can encounter in their life-cycles. Low velocity impact damage mainly consists of matrix cracks followed by delaminations at the ply interfaces. Impact damage below the detectability threshold (barely visible impact damage, BVID) formed within the laminate may propagate during aircraft flight cycles, leading to a

*Corresponding author : Aravind Sasikumar, Josep Costa
Email addresses: aravind.sasikumar@udg.edu (A.Sasikumar), josep.costa@udg.edu (J.Costa)
[1] Serra Hunter Fellow

major reduction in residual strength [1], especially the compression after impact (CAI) strength. During CAI loading, the formed delaminations tend to propagate and split the laminate into sub-laminates, and these thinner sub-laminates buckle easily, leading to final failure. In the case of standard thick laminates (4-5 mm), delamination induced buckling is the critical phenomenon causing structural collapse under compression, whereas in the case of thin laminates (1-2 mm), impact induced fibre failure triggers final laminate failure [2; 3].

In the quest to improve CAI strength, numerous researchers [4–6] initially tried to understand the relationship between impact damage and CAI strength. They studied the effect various damage parameters such as projected damage area [7], delamination threshold load [8] and impact dent depth [9] had on CAI strength. Because of unclear conclusions, researchers subsequently focussed on delamination parameters such as the through-the-thickness delamination position, orientation and size [10–13] and the associated laminate buckling modes [14] and how they affect CAI strength. Hu et al. [15] performed compressive numerical buckling analysis with one embedded delamination and reported that the buckling load increased significantly as the position of the delamination approached the laminate mid-plane due to the change in the buckling mode from a local to a global one. A similar conclusion was reported by Butler et al. [16] using an analytical model. They stated that deep sited delaminations were safe as they opened under compressive loading and would not grow to cause failure. Despite these interesting conclusions, in a real impact scenario the effect on CAI strength could be completely different due to the development of many more damage forms.

Apart from applying material reinforcement methods [17], researchers have also pushed the laminate design boundaries to propose non-conventional stacking sequences, such as varying mismatch angled interfaces [18; 19], complete [19; 20] or localized ply clustering [21], or dispersed ply orientations [22–24] in an attempt to tailor the impact damage resistance and improve the CAI strength. Liv et al. [19] demonstrated that complete clustering of plies ($[90_3/-45_3/0_3/45_3]_s$) led to a decreased impact resistance and a 15% lower CAI strength compared to a non-clustered baseline ($[90/45/-0/-45]_{3s}$). This was mainly attributed to the wide extended delaminations adjacent to the ply clusters. However, Sebaey et al. [21] using dispersed ply orientations and localized clusters of 0° plies, reported an improvement in CAI strength over the baseline quasi-isotropic laminate.

Reviewing the damage morphology, low velocity impact induces damage modes that are unsymmetrical in the through-the-thickness direction of the laminate [1; 25]. Despite both the loading and the damage being unsymmetrical in the laminate, the conventional mid-plane symmetry constraint is still followed. In response, the authors [26] proposed warp-free unsymmetrical laminates (with the extensional-bending coupling matrix B=[0]) with localized ply clusters placed only on the impacted side of the laminate. The same laminate, when flipped upside down, led to another unsymmetrical laminate with clustered plies on the non-impacted side of the laminate. Experimental (low velocity impact and quasi-static indentation tests) and numerical studies on the two laminates concluded that (a) delaminations can be tailored to occur at pre-determined locations and (b) unsymmetrical stacking designs offer a promising prospect for unsymmetrical loading conditions. Despite demonstrating that impact damage can be tailored, the study lacked the crucial information of the resulting compressive strength (CAI) and a comparison with a symmetric baseline in terms of impact resistance and CAI strength.

Hence, in this paper we propose three unsymmetrical laminates, where local ply clusters are placed at the impacted side, the middle of the laminate and the non-impacted side, and a reference symmetric baseline laminate (with no ply clusters). Using low velocity impact, micro computed X-ray tomography inspections and CAI tests, we compare the impact resistance, damage evolution and CAI strengths of all four laminates. The objective of the study is twofold: (a) to understand the effect the local ply clusters, their location in the laminate, and the location of the dominant delaminations (imposed by the clusters) have on the CAI strength and (b) to compare the damage tolerance of the proposed non-conventional unsymmetrical laminates to that of the symmetric baseline laminate (as suggested in ASTM standards [27]) to assess the prospects of the unsymmetrical laminate designs. According to the authors' knowledge, this is the first report of a comparison between conventional symmetric laminate and nonconventional unsymmetrical laminates in the framework of impact damage and CAI strength.

2. Laminate design

2.1. Optimization

Different laminates with local ply clusters at the impacted side, the middle of the laminate and the non-impacted side were designed. Because the clusters were placed only at particular locations in the laminate, this meant violating the conventional mid-plane symmetry constraint and therefore leading to unsymmetrical laminate solutions. Since unsymmetrical laminates can induce coupling responses under loading (due to the presence of non-zero extensional-bending coupling matrix ([B]) [28]), such as warping during the curing process, optimization methods were used to obtain unsymmetrical laminates with zero or close to zero B matrix terms.

Using a genetic algorithm from MATLAB [29], we obtained three unsymmetrical laminates (two that had already been proposed in the previous work [26]) with clustered ply blocks placed at the top, the middle or the bottom of the laminates. Note that top refers to the impacted side and bottom refers to the non-impacted side of the laminate. The objective function was set to minimize the summation of the B matrix terms to avoid undesired coupling responses. In addition, the following constraints were also included: (a) the laminate had to be quasi-isotropic and balanced with 24 plies in total, (b) four clustered ply blocks (one cluster for each ply orientation i.e., 0°, ±45° and 90°) were placed at the respective desired location (top/middle/bottom) to impose delamination damage at that location; (c) no more than three plies of the same orientation were placed together, (d) outer laminate plies were fixed to be either 45° or -45° to counteract the shear loads [22], and (e) the equivalent bending stiffness parameter D* of the proposed laminates were to match within 5% that of the baseline laminate (D* was proposed by Olsson [30; 31] to ensure proper comparisons between laminates, as was also implemented in [32]).

2.2. Laminates

The unsymmetrical laminate obtained with local ply clusters at the impacted side (top side) is referred to as LPCI, while the same flipped laminate with ply clusters at the non-impacted side (bottom side) is referred to as LPCN (as presented in [26]). Finally, the unsymmetrical laminate with ply clusters at the middle of the laminate is hereafter referred to as LPCM. Note that LPCI and LPCN have null B matrices while LPCM has low but non-zero B matrix terms (with a maximum term of 2 kPa.m^2). In addition, we introduce a symmetric laminate (as recommended in the ASTM standard [27]) as the baseline comparison case. Table 1 details the stacking sequences and Fig. 1 provides an illustration of all four laminates and the through-the-thickness location of the ply clustered blocks. Fig. 2 (a) and (b) represent the polar plot of the in-plane and bending stiffness, respectively, of all the laminates. It is important to note that all the laminates are in-plane quasi-isotropic with equal ply counts in all the orientations. All the laminates have the same number of 0° plies, thus assuring a fair comparison for CAI strength which is measured at 0°. The equivalent bending stiffness values of LSYM, LPCI, LPCN and LPCM are 373.9, 372.2, 372.2 and 373.1 Nm, respectively, and the values of the proposed laminates fall within 1% of that of the baseline laminate. The bending stiffnesses of all three unsymmetrical laminates in the 0° and 90° directions are the same.

[Figure 1 about here.]

[Table 1 about here.]

[Figure 2 about here.]

3. Experimental methods

The material used was IM7/M21 prepreg uni-directional tape, and the panels were cured in an autoclave. Impact specimens of 150 x 100 mm were cut out from the panel with 0° fibres aligned in the direction of the specimen length. The unsymmetrical laminates had no warping, with respect to the zero or low values of the B matrix. With a ply thickness of 0.184 mm and 24 plies, all the laminates resulted in a nominal thickness of 4.41 mm. The LPCI specimens were flipped upside down to obtain LPCN laminates. In accordance with ASTM D7136/D7136-M standards [27], impact tests were performed on the 150 x 100 mm specimens using a CEAST Fractovis Plus instrumented drop-weight tower. A total of four impact energies were explored: 10, 16, 24, and 35 J, with three specimens per laminate tested for each impact energy. The range of impact energies was selected such that the lowest energy induces minimum damage in order to understand the damage initiation process, while the higher energies lead to barely visible impact damage and extended delaminations inside the laminate. Impact specimens were placed over a metallic fixture base with a rectangular cut out of 125 x 75 mm, and four rubber tipped clamps restrained the specimen during impact. A 16 mm in diameter hemispherical tip impactor, with a 5 kg impactor setup mass was used for all the tests in the study. For further details of the test setup, refer to [20; 33].

All the impacted specimens were subjected to compression using an MTS INSIGHT 300 machine with a 300 kN load cell, following the ASTM D7137/D7137-15 [34] in order to obtain the compression after impact strength. The impacted specimen is placed between flat plates in the test fixture, and end-loaded under compression to obtain a compressive failure induced by the impact damage (refer to [33] for details of the test fixture). To measure the out-of-plane displacements and study the buckling modes, we placed two LVDT sensors, one each at the centre of the impacted and non-impacted sides of the impacted specimen. Furthermore, to evaluate the pristine compression strength, plain compression strength tests were performed in accordance with the ASTM D6641/D6641M-16 [35]. The compressive force is introduced into the specimen by combined end- and shear-loading and the specimens were tabbed leaving a 13 mm tab free region in the centre (refer to [33] for more details). Five 140 x 13 mm specimens per laminate were tested under plain compression, and both compression tests above were performed with a cross head displacement of 0.5 mm/min.

The impact damage in all the laminates were inspected using a pulse-echo ultrasonic C-scan technique. We used an OLYMPUS OMNI MX system equipped with a 5 MHz piezoelectric probe. The specimens were immersed in a water pool and the probe's movement was controlled by an automatized robotic arm (Refer to [33] for the details). Furthermore, one of the 10 J impacted specimens per laminate was subjected to an X-ray micro-computed tomography (μCT) inspection. Before the inspection, the impact specimens were cut into 30 mm wide strips (with the impact point as the centre), making sure that all the impact damage was within this strip (determined by C-scan inspection). Using laminate strips instead of the whole impact specimen was done to minimize the unwanted X-ray absorption perpendicular to the axis of rotation as reported in [36]. The scanning parameters were: 50 kV, 175 μA, 1400 projections with three integrations per projection, an effective pixel size of 10 μm with a field of view of approximately 22 mm and the inspection time was two and a half hours per specimen. The μCT slices were post-processed using Matlab [29] and 3D rendered in Starviewer software [37], where we differentiated matrix cracks and delaminations in the final 3D image. For more details of the inspection equipment and the post-processing of the slices, the reader can refer to [36; 38]. All the above-mentioned tests and inspections were performed at the AMADE research laboratory, which is NADCAP certified for non-metallic material testing, at the University of Girona.

4. Results

4.1. Impact responses

Figs. 3, 4 and 5 represent the force-time, force-deflection and energy-time responses of all the four laminates for all the impact energies, respectively. Due to the excellent repeatability in the impact responses, only one specimen data per impact energy per laminate is shown. The figures convey that the global impact responses of all four laminates are quite similar, mainly in terms of their maximum peak forces, impact response times and the energy evolution (in Figs. 3 and 4). Despite their similar responses, the delamination threshold loads (F_d) differ between the laminates. With LSYM as the baseline, laminate LPCN exhibited an early delamination initiation (13% reduction in the delamination threshold load), while LPCI and LPCM increased the threshold load by 7% and 5%, respectively, over LSYM (as in Fig. 3 (c)).

[Figure 3 about here.]

[Figure 4 about here.]

[Figure 5 about here.]

Figs. 6 (a) and (b) present the maximum peak loads and projected damage areas, respectively, for all the laminates. As previously mentioned, the peak loads are roughly the same for all the laminates throughout the entire range of energies, thus indicating the similar load carrying capability the four laminates have, despite the presence of clusters in the unsymmetrical laminates. However, this is not the case with the projected damage area. On comparing all four impact energies, the baseline LSYM exhibited the least damage area whereas LPCN exhibited the highest. For the lower impact energies (10 J and 16 J), LSYM and LPCM exhibited roughly the same damage areas. For higher energies, LPCM exhibited a 50% higher damage area, while LPCI showed a 60% more damage area than the baseline. Throughout all the impact energies, LPCN exhibited more than twice the damage area as that of LSYM.

Figs. 7 (a) and (b) show the dissipated energies and impact dent depths, respectively, of all the laminates for all impact energies. For the lowest energy, 10 J, all the laminates dissipated roughly the same amount of energy. In the cases of 16 J and 24 J, all three unsymmetrical laminates exhibited roughly the same dissipated energy (around 10% higher than LSYM), whereas for the highest energy, 35 J, LSYM exhibited the least and LPCI dissipated the highest (18% higher than LSYM). Of the three unsymmetrical laminates, LPCM dissipated the least energy considering all the energies. In view of the impact dent depth, laminates LSYM and LPCI displayed similar dent depth values, whereas LPCN exhibited the highest for all the impact energies. For the highest impact energy, LPCM and LPCN displayed approximately 25% higher dent depth compared to the baseline LSYM.

[Figure 6 about here.]

[Figure 7 about here.]

4.2. Impact damage inspection

Fig. 8 presents the damage footprint (matrix cracks and delaminations) of all the laminates obtained from the post-processed μCT slices of the lowest impact energy (10 J). Using the same field of view for all the laminates, LPCN clearly exhibits a higher projected damage area, whereas LPCM displays the least. LSYM and LPCI exhibit similar projected damage contours with similar areas.

[Figure 8 about here.]

The projected damage presented above has been extruded in the laminate thickness direction to present a 3D view of the damage (Fig. 9) in order to: (a) identify whether the local ply clusters have induced delamination at their respective locations, and (b) understand and compare the different damage modes in the thickness direction between all the laminates. The laminates are presented as three sub-laminates where SL-1, SL-2 and SL-3 represent the top, middle and bottom sub-laminates. The clustered blocks, which consists of 9 plies, of the unsymmetrical laminates are grouped as one sub-laminate and are represented by a green box for easy comparison.

LSYM and LPCI displayed similar damage patterns when the three sub-laminates of both laminates are compared. Both laminates had their dominant delaminations in the sub-laminate closest to the non-impacted side (SL-3). Note that with LPCI, the clustered plies are in SL-1 and the dominant delaminations are found in SL-3, contrary to the prediction we made in the laminate design phase. As mentioned earlier, LPCN showed the highest projected damage and it is evident from the 3D view that all the damage is concentrated in the sub-laminate SL-3 (closest to non-impacted side), i.e., the sub-laminate where clustered plies were imposed. The delaminations within these interfaces (int. 15, 16, 17 and 18 as given in Fig. 1) have extended to the boundaries of the inspected field of view; something not observed in any other laminate. Finally, the LPCM laminate was found to have the least amount of damage when compared with all the sub-laminates (SL-1, SL-2, and SL-3) of all four laminates. The dominant delamination was found in the clustered plies sub-laminate (SL-2), oriented in the 0°

direction (int 10: (45/0), delamination marked by green). Note that all the laminates exhibited matrix cracks at the impacted surface (shown in black colour in the SL-1 sub-laminates) around the vicinity of the impactor.

[Figure 9 about here.]

Moving to the higher impact energies, Fig. 10 presents the images of the C-scan inspection (from the impacted face) of all the laminates for 16, 24 and 35 J impact energies. The dominant delaminations identified as well as the projected damage areas, are marked in the same figure. Compared to the proposed unsymmetrical laminates, the symmetric baseline laminate, LSYM, exhibited the least damage area for all the energies. Furthermore, due to the contribution of the different delaminations, it was difficult to pinpoint particular dominant delaminations. Moving to LPCI, lower energy 16 J produced a similar damage footprint as that of LSYM, but at higher energy levels the delamination at the clustered zone (Int 3: ($45_2/0_3$), oriented in the 0° direction) became prominent. LPCN displayed the largest projected damage area compared to other laminates, and dominant delaminations were identified at the last three bottom interfaces (Int 16, 17 and 18), at the site of the clustered block. Out of the three unsymmetrical laminates, LPCM exhibited the lowest damage area, and from 24 J to 35 J, the dominant delaminations were found within the clustered zone (Int 10 ($-45_2/0_3$)) and below the cluster (Int 14 (-45/90)).

[Figure 10 about here.]

4.3. Compression after impact

Fig. 11 (a) presents the pristine compression strengths along with the CAI strengths of all the laminates for increasing impact energies. Fig. 11 (b) depicts the compression strengths normalized with respect to the baseline LSYM. All three unsymmetrical laminates exhibited slightly higher plain compression strength over the baseline LSYM (LPCN and LPCI by 3% and LPCM by 7%). For the 10 J energy, LPCM exhibited the highest CAI strength out of all laminates (10% higher than the baseline LSYM), whereas LPCN exhibited the lowest (5% lower than LSYM). Moving to 16 J, LPCI showed a sudden drop in the CAI strength (from an increase of 5% for 10 J to an 8% reduction for 16 J, over the baseline LSYM). Both LPCI and LPCN showed reduced CAI strength over LSYM for the 16 J impact. Over the entire impact energy range, LPCM exhibited higher CAI strength than LSYM by an average of 8%. It should be noted that even though LPCN exhibited lower CAI strength for the first two impact energies, for the last two energies, LPCN showed the same CAI strengths as those of the baseline LSYM. On comparing the three unsymmetrical laminates, LPCM (laminate with the ply cluster in the middle) displayed higher CAI strength over the other two laminates (15% over LPCI and 10% over LPCN, considering the last three energy levels). Fig. 12 shows the normalized reduction (with respect to the pristine strength) in compression strength due to the impact damage for different impact energies. Almost similar strength reductions were observed with all the laminates, with LPCI exhibiting the highest reduction in residual strength, by around 60% for the higher impact energies.

[Figure 11 about here.]

[Figure 12 about here.]

Fig. 13 displays the macro photos of the failed CAI specimens' edge for all the laminates from the highest impact energy. The compression loading direction is represented in the figure and note that all the laminates are presented such that the impacted side of the specimen is at the top. In addition, the through-the-thickness location of the clustered block is marked by a yellow box for all unsymmetrical laminates. The dominant delaminations from the impact have propagated to the specimen edge and are seen in the figure. While in LPCI, the dominant delamination in the clustered block (at the top) is seen to have propagated and created a sub-laminate, the same is seen with the bottom delaminations of LPCN. In the case of LPCM, delamination close to the laminate mid-plane has reached the specimen edge. Hence, it is evident that the dominant delaminations (formed during impact damage) located at the imposed clustered plies have propagated to the specimen edges to create sub-laminates during CAI loading (as reported in [6]).

[Figure 13 about here.]

Fig. 14 presents the evolution of the out-of-plane displacements of the LSYM and LPCM laminates obtained from LVDT-1 and LVDT-2 (placed at the centre of the impacted and non-impacted sides, respectively) during the CAI test of the 16 J impact. LVDT readings confirm that both laminates, LSYM and LPCM, buckled towards the non-impacted side during the CAI loading. LSYM buckled progressively towards the non-impacted side and finally led to the collapse of the laminate marking a maximum out-of-plane displacement of 0.2 mm. In the case of LPCM, at lower CAI loads (around 30 KN), there is a higher out-of-plane displacement compared to LSYM. But with increased loading, there is a saturation in the displacement value, evidence of the laminate resisting buckling. At the failure load, the out-of-displacement observed is roughly similar to the value seen at lower CAI loads. Furthermore, the final out-of-plane displacement value at the point of laminate failure is four times lesser for LPCM compared to LSYM. LPCI showed similar out-of-displacement values as LSYM but buckled globally towards the impacted side. LPCN behaved differently with respect to the impact energy levels. For the lower energy levels, LPCN showed an open buckling mode where the impacted side and non-impacted side buckled towards the respective sides. Meanwhile for the higher energies it buckled as a whole towards the impacted side.

[Figure 14 about here.]

5. Discussion

5.1. Impact damage analysis

During an impact, the laminate bends towards the non-impacted side which introduces in-plane tensile stresses in the bottom plies. The tensile loads induce transverse matrix cracks in the bottom plies, and, in addition, due to bending, the bottom interfaces are subjected to higher interlaminar shear stresses. The transverse tensile cracks and the shear cracks link up in the through-the-laminate thickness to induce delamination. Hence, in a conventional impact damage morphology, the laminate exhibits a spiral stair-case delamination pattern (as reported in [1; 39]), where the delaminations are extended in the bottom interfaces and are reduced towards the impacted side. This is similar to what is seen in LSYM and LPCI for the 10 J impact case from the post-processed tomography images (Figs. 8 and 9). In addition, the existence of an undamaged cone under the impactor, as observed in [7], is evident in all the laminates studied (Fig. 9).

Further, when the similar oriented plies are clustered, they introduce a higher bending stiffness mismatch [40] and thereby higher interlaminar shear stresses at the adjacent interfaces compared to the non-clustered ply interfaces. Moreover, the transverse cracking is less constrained in the thicker plies (i.e., clustered) compared to the non-clustered, due to the in-situ effect [41]. Hence, as explained above, the bottom interfaces of the laminate are more prone to having extended delaminations compared to other locations, and clustering the plies at the bottom (as in laminate LPCN) serves as a catalyst to the already prone delaminations at the bottom. These bottom-clustered plies act as a source of early initiation of cracks and delamination and hence the delamination threshold load was seen to be the least for LPCN (as in Fig. 4). This also explains the reason behind the large extended delaminations found in the bottom sub-laminate for LPCN compared to the other laminates (Figs. 9 and 10).

In the case of LPCI (where the localised cluster is placed in the top sub-laminate), the lowest energy level 10 J failed to impose dominant delaminations at the top of the laminate (as was expected during the laminate design phase). Nevertheless, they were seen at the bottom sub-laminate similar to the case of LSYM. This is due to the effect of local through-the-thickness compressive stresses right under the impactor that delay the delamination by increasing interlaminar shear strength and mode II fracture toughness [26; 42–44]. However, for the higher impact energies, the C-scans inspections (Fig. 10) reveal that the dominant delaminations are formed at the location of the clustered plies, as the delaminations have extended outside the local compressive region thereby counterbalancing the effect of the local compressive stresses.

On the other hand, LPCM (where the cluster is in the middle of the laminate) also followed the predictions of the laminate design (delamination was observed at the middle sub-laminate, Fig. 9), even though smaller, but significant delaminations, were found in the bottom sub-laminate too. The delaminations induced by the clusters in the mid-plane have significantly reduced or even avoided the delaminations at the top and bottom sub-laminates, when compared to the other three laminates. At higher energies, the delaminations within the clustered zone were prevalent, as evidenced by the C-scan images. Hence, the idea of forcing delamination to occur at desired places through laminate design techniques is demonstrated. Similar observations of forcing delaminations were reported in [19; 21] using laminate stacking sequence designs.

Despite the similar impact response curves by all the laminates for all the impact energies, the increased projected damage area for the unsymmetrical laminates over the symmetric baseline laminate is a result of the effect local clustered plies have. The effect the through-the-thickness delamination location has on impact resistance is evidenced by LPCM's reduced damage area and dissipated energy.

5.2. Effect of local ply clusters and delamination location on CAI strength

The small improvement in the plain compression strength of the unsymmetrical laminates over the baseline (Fig. 11) signifies that the thicker plies (or clustered plies), mainly the $0°$ plies, help in effectively carrying the compressive load. Further, the effect of the position of the local cluster is also significant as the laminate with the cluster at the middle showed higher compression strength over the ones with the clustered blocks placed at the specimen surfaces (top or bottom as in LPCI and LPCN, respectively). LPCM improved the CAI strength over LSYM due to the effect of clustered plies (mainly $0°$ plies) and the mid-plane location of the dominant delaminations it imposed. The lower CAI strength of LPCN and LPCI over LPCM shows that delaminations closer to the mid-plane resist buckling compared to the surface delaminations under compression loading. This is in line with the conclusions from the numerical studies in [6; 15], which reported that near surface delaminations induced buckling at lower loads. Nevertheless it should be noted that despite understanding the significant effect of delamination location on the CAI strength, other factors such as the thickness and orientation of the other plies, laminate thickness, material system etc. play a significant role too, whose effect is not discussed in this study.

The LPCN laminate exhibited different buckling modes depending on the impact energies. For lower energies, the dominant delaminations of LPCN at the bottom split the bottom sub-laminate from the rest of the laminate, and the plies within this sub-laminate easily buckled outwards to the non-impacted side. But for higher energies, the same bottom sub-laminate buckled inwards to the impacted side where the intact top sub-laminate helps resist and delay the final failure. This could be the reason behind the lesser reduction in the CAI strength of LPCN (almost the same CAI strength as LSYM at 24 and 35 J) when moving from lower to higher energies.

Similarly with LPCI, the dominant delaminations split the laminate where the clustered block at the top can easily buckle outwards due to the reduced stiffness of the sub-laminate. In the case of

LPCM, the out-of plane displacements suggest that there was initial global buckling towards the non-impacted side, but that the delamination propagation split the laminate into sub-laminates with the intact clustered block taking the compression load (Fig. 13). In addition, this cluster of plies (especially the 0° plies) resisted buckling (as also reported in [45]) because of the surrounding plies at the top and bottom. This is in agreement with the results reported in [21; 45], where clustered plies improved the damage tolerance through reduced buckling. Hence, it was the compressive failure of the main load-bearing plies that triggered the final CAI collapse (as evidenced in Fig. 14). This alternative failure mechanism of compressive fibre fracture because of the buckled plies was also reported in [46]. It is worth remarking that even though complete clustering of a laminate was reported to impair the impact resistance and damage tolerance [19; 20], clustering plies locally is observed as being advantageous in this study (as also reported by Sebaey et al. [21]).

5.3. Damage resistance parameters v/s CAI strength

The similar impact response curves of the different laminates elucidate the effectiveness of the laminate design study where the laminates were designed to have similar in-plane and bending responses for fair comparison. Since all four laminates have similar impact responses, it holds this as a fair platform from which the correlation of different impact resistance parameters on CAI strength can be studied. Aircraft manufacturers still use projected damage area to correlate CAI strength, where a higher area denotes less CAI strength. From this study, it is clear that projected damage area is a very misguiding parameter to relate CAI strength to, as also observed in [2]. For the highest impact energy, LPCN showed 115% increased damage area compared to the baseline LSYM, but both laminates showed similar CAI strength values. Similarly, the unsymmetrical laminate, LPCM, showed 7% higher CAI strength despite having 55% higher projected damage area over LSYM for the 35 J impact. A similar trend is seen for dissipated energy, where the lower dissipated energy of LSYM did not proportionate to a higher CAI strength. Moreover, it is also observed that if a laminate has a higher resistance to the onset of delamination (LPCI in this case), this does not imply a higher CAI strength. LPCI delayed delamination onset and LPCN exhibited early delamination onset, but finally LPCN displayed higher CAI strength over LPCI. Hence, it is clear that CAI damage morphology is too complex to be predicted or correlated with the impact resistance parameters. The final failure is seen to depend more on the through-the-thickness position of the dominant delamination, the thickness of the sub-laminates formed during CAI loading and the buckling modes of the sub-laminates, rather than simply just the damage resistant parameters (as discussed above).

From an industrial point of view, the damage tolerance concept suggests that the structure should have enough strength to continue in service until the damage is detected by a scheduled inspection. A dent depth greater than 0.25 mm has greater probabilities of being detected during a visual inspection

[47], and the corresponding energy level is termed as BVID energy level. Hence, in combining the laminate residual strength and the damage detectability, laminates LPCM and LPCN displayed higher dent depth (BVID energy level of 24 J) than LSYM and LPCI (BVID energy level of 36 J). Thus, despite having higher (as for LPCM) or equal (as for LPCN) CAI strengths compared to LSYM, the chances of detecting the damage in LPCM or LPCN are also greater compared to LSYM. The worst case is when the cluster is placed at the impacted side (as in LPCI), where the CAI strength and the chances of detecting the damage are the lowest, leading to a critical situation.

5.4. The prospects of unsymmetrical laminates

Using warp-free unsymmetrical stacking sequences, we have exhibited the capability to improve the damage tolerance compared to the standard ASTM baseline laminate. It should be kept in mind that even though the improvement is not dramatic, it was achieved economically by simply clustering some plies and through an unsymmetrical design (without reinforcing the material system or using dispersed ply orientations [21; 22]). That said and putting this improvement to one side, the different unsymmetrical laminates helped to obtain a clear understanding of the effect delamination position has on CAI strength, which until now had been missing, despite the conclusions reported from numerical and analytical studies [15; 16].

With the objective to investigating the CAI response of unsymmetrical laminates and their comparison with a symmetric baseline laminate) missing from the previous work [26], this study demonstrates that symmetric laminates are not the optimal damage tolerant solution to impact loading cases. A similar conclusion was reported by Baker et al. [48] supporting the idea of unsymmetric laminate design.

In instances such as aircraft skins, unsymmetrical laminates may be a promising solution (e.g., for higher impact damage tolerance or higher electrical conductivity). Furthermore, unsymmetrical laminates can be looked upon as being an option to design hybrid laminates tailored for impact loads (as performed by the authors with thin laminates [32]), where the plies on the impacted side can be designed with thick plies and the non-impacted side with thin plies, thereby mitigating the critical delamination damage at the non-impacted side using thin plies.

6. Conclusion

This study extends the findings of a previous work [26] on unsymmetrical laminates tailored for impact resistance by evaluating the compression after impact strength and providing a comparison with a symmetric baseline laminate. In this paper, we designed three warp-free unsymmetrical laminates to have local ply clusters placed at the impacted side, middle and non-impacted side of the respective laminates, with the aim of imposing delaminations at these particular through-the-thickness locations.

By means of low velocity impacts, X-ray tomography and ultrasonic C-scan inspection of the impacted specimens and compression after impact tests, we compared the impact responses, damage and the compression after impact strengths to that of a symmetric baseline laminate. The site of dominant delaminations at the location of clustered plies in the unsymmetrical laminates supports the concept that damage can be imposed at desired locations through laminate design. Despite the reduced impact resistance (50% increased damage area and 10% higher energy dissipated) over the baseline laminate, the unsymmetrical laminate with ply clusters at the middle improved CAI strength by 10%. The same laminate with delamination in the middle buckled the least under CAI (four times lesser out-of-plane displacements compared to symmetric baseline laminate) and increased the failure load (by 15%) over the other unsymmetrical laminates with delamination at the outer surfaces. We demonstrated that unsymmetrical over symmetrical laminates can offer improved CAI strengths and can be an optimal solution for application in structures such as aircraft skins.

Acknowledgements

The first author would like to thank the Generalitat de Catalunya for the FI-DGR pre-doctoral grant (2018 FI-B2 00118). The authors would like to thank the *Spanish Ministerio de Ciencia, Innovacíon y Universidades* for the grants coded RTI2018-097880-B-I00 and RTI2018-099373-B-I00. We would like to acknowledge *Instituto Nacional de Técnica Aeroespacial* (INTA), Madrid, Spain for manufacturing all the specimens used in this study. We also acknowledge the support of Dr. Imma Boada and her team (Graphics and Imaging Laboratory, University of Girona) for providing the Starviewer software that was used to 3D render the tomographic slices.

References

[1] S. Abrate, Impact on composite structures, Cambridge University Press, 2005.

[2] A. Sasikumar, D. Trias, J. Costa, J. Orr, P. Linde, Effect of ply thickness and ply level hybridization on compression after impact strength of thin laminates, Composites Part A: Applied Science and Manufacturing 121 (2019) 232–243.

[3] A. Sasikumar, D. Trias, J. Costa, N. Blanco, J. Orr, P. Linde, Impact and compression after impact response of thin laminates of spread-tow woven and non-crimp fabrics, Composite Structures 215 (2019) 432–445.

[4] M. Abir, T. Tay, M. Ridha, H. Lee, On the relationship between failure mechanism and compression after impact (CAI) strength in composites, Composite Structures 182 (2017) 242–250.

[5] T. Sebaey, E. González, C. Lopes, N. Blanco, J. Costa, Damage resistance and damage tolerance of dispersed CFRP laminates: Design and optimization, Composite Structures 95 (2013) 569–576.

[6] Y. Liv, A contribution to the understanding of compression after impact of composite laminates, PhD thesis, University of Girona; 2017.

[7] D. Bull, S. Spearing, I. Sinclair, Observations of damage development from compression-after-impact experiments using ex-situ micro-focus computed tomography, Composites Science and Technology 97 (2014) 106–114.

[8] D. Cartie, P. Irving, Effect of resin and fibre properties on impact and compression after impact performance of CFRP, Composites part A: Applied Science and Manufacturing 33 (4) (2002) 483–493.

[9] S. Petit, C. Bouvet, A. Bergerot, J.-J. Barrau, Impact and compression after impact experimental study of a composite laminate with a cork thermal shield, Composites Science and Technology 67 (15-16) (2007) 3286–3299.

[10] M. A. Kouchakzadeh, H. Sekine, Compressive buckling analysis of rectangular composite laminates containing multiple delaminations, Composite Structures 50 (3) (2000) 249–255.

[11] A. T. Rhead, R. Butler, N. Baker, Analysis and compression testing of laminates optimised for damage tolerance, Applied Composite Materials 18 (1) (2011) 85–100.

[12] S.-F. Hwang, S.-M. Huang, Postbuckling behavior of composite laminates with two delaminations under uniaxial compression, Composite Structures 68 (2) (2005) 157–165.

[13] V. Obdržálek, J. Vrbka, On buckling of a plate with multiple delaminations, Engineering mechanics 17 (1) (2010) 37–47.

[14] L. Reis, M. De Freitas, Damage growth analysis of low velocity impacted composite panels, Composite Structures 38 (1-4) (1997) 509–515.

[15] N. Hu, H. Fukunaga, H. Sekine, K. M. Ali, Compressive buckling of laminates with an embedded delamination, Composites science and technology 59 (8) (1999) 1247–1260.

[16] R. Butler, D. P. Almond, G. Hunt, B. Hu, N. Gathercole, Compressive fatigue limit of impact damaged composite laminates, Composites Part A: Applied Science and Manufacturing 38 (4) (2007) 1211–1215.

[17] S. García-Rodríguez, J. Costa, V. Singery, I. Boada, J. Mayugo, The effect interleaving has on thin-ply non-crimp fabric laminate impact response: X-ray tomography investigation, Composites Part A: Applied Science and Manufacturing 107 (2018) 409–420.

[18] T. Sebaey, E. González, C. Lopes, N. Blanco, P. Maimí, J. Costa, Damage resistance and damage tolerance of dispersed CFRP laminates: Effect of the mismatch angle between plies, Composite Structures 101 (2013) 255–264.

[19] Y. Liv, G. Guillamet, J. Costa, E. González, L. Marín, J. Mayugo, Experimental study into compression after impact strength of laminates with conventional and nonconventional ply orientations, Composites Part B: Engineering 126 (2017) 133–142.

[20] E. González, P. Maimí, P. Camanho, C. Lopes, N. Blanco, Effects of ply clustering in laminated composite plates under low-velocity impact loading, Composites Science and Technology 71 (6) (2011) 805–817.

[21] T. Sebaey, E. González, C. Lopes, N. Blanco, J. Costa, Damage resistance and damage tolerance of dispersed CFRP laminates: Effect of ply clustering, Composite Structures 106 (2013) 96–103.

[22] C. Lopes, O. Seresta, Y. Coquet, Z. Gürdal, P. Camanho, B. Thuis, Low-velocity impact damage on dispersed stacking sequence laminates. Part I: Experiments, Composites Science and Technology 69 (7-8) (2009) 926–936.

[23] C. Lopes, P. Camanho, Z. Gürdal, P. Maimí, E. González, Low-velocity impact damage on dispersed stacking sequence laminates. Part II: Numerical simulations, Composites Science and Technology 69 (7-8) (2009) 937–947.

[24] A. Wagih, P. Maimí, N. Blanco, S. García-Rodríguez, G. Guillamet, R. Issac, A. Turon, J. Costa, Improving damage resistance and load capacity of thin-ply laminates using ply clustering and small mismatch angles, Composites Part A: Applied Science and Manufacturing 117 (2019) 76–91.

[25] A. Wagih, P. Maimí, N. Blanco, J. Costa, A quasi-static indentation test to elucidate the sequence of damage events in low velocity impacts on composite laminates, Composites Part A: Applied Science and Manufacturing 82 (2016) 180–189.

[26] A. Sasikumar, J. Costa, D. Trias, E. V. González, S. García-Rodríguez, P. Maimí, Unsymmetrical stacking sequences as a novel approach to tailor damage resistance under out-of-plane impact loading, Composites Science and Technology 173 (2019) 125–135.

[27] ASTM D7136/D7136-15, Standard test method for measuring the damage resistance of a fiber reinforced polymer matrix composite to a drop weight impact event, 2015.

[28] R. M. Jones, C. Bert, Mechanics of composite materials (1975).

[29] MATLAB, version 8.5.0 (R2015a), The MathWorks Inc., Natick, Massachusetts, 2015.

[30] R. Olsson, Mass criterion for wave controlled impact response of composite plates, Composites Part A: Applied Science and Manufacturing 31 (8) (2000) 879–887.

[31] R. Olsson, Closed form prediction of peak load and delamination onset under small mass impact, Composite Structures 59 (3) (2003) 341–349.

[32] A. Sasikumar, D. Trias, J. Costa, V. Singery, P. Linde, Mitigating the weak impact response of thin-ply based thin laminates through an unsymmetrical laminate design incorporating intermediate grade plies, Composite Structures 220 (2019) 93–104.

[33] A. Sasikumar, Improving compression after impact response of composite laminates through ply level hybridization with thin plies and unsymmetrical designs, PhD thesis, University of Girona; 2019.

[34] ASTM D7137/D7137-15, Standard Test Method for Compressive Residual Strength Properties of Damaged Polymer Matrix Composite Plates, 2015.

[35] ASTM D6641/D6641M-16, Standard test method for compressive properties of polymer matrix composite materials using a combined loading compression (CLC) test fixture, 2016.

[36] S. García-Rodríguez, J. Costa, A. Bardera, V. Singery, D. Trias, A 3d tomographic investigation to elucidate the low-velocity impact resistance, tolerance and damage sequence of thin non-crimp fabric laminates: effect of ply-thickness, Composites Part A: Applied Science and Manufacturing 113 (2018) 53–65.

[37] Starviewer medical imaging software, http://starviewer.udg.edu.

[38] S. García-Rodríguez, J. Costa, P. Maimí, V. Singery, A. Sasikumar, On how matrix cracks induce delamination under out-of-plane shear and the associated in-situ effect, Submitted to Composites Science and Technology (2019).

[39] M. Wisnom, The role of delamination in failure of fibre-reinforced composites, Philosophical Transactions of the Royal Society A: Mathematical, Physical and Engineering Sciences 370 (1965) (2012) 1850–1870.

[40] D. Liu, Impact-induced delamination—a view of bending stiffness mismatching, Journal of Composite Materials 22 (7) (1988) 674–692.

[41] P. P. Camanho, C. G. Dávila, S. T. Pinho, L. Iannucci, P. Robinson, Prediction of in situ strengths and matrix cracking in composites under transverse tension and in-plane shear, Composites Part A: Applied Science and Manufacturing 37 (2) (2006) 165–176.

[42] X. Li, S. R. Hallett, M. R. Wisnom, Predicting the effect of through-thickness compressive stress on delamination using interface elements, Composites Part A: Applied Science and Manufacturing 39 (2) (2008) 218–230.

[43] G. Catalanotti, C. Furtado, T. Scalici, G. Pitarresi, F. Van Der Meer, P. Camanho, The effect of through-thickness compressive stress on mode ii interlaminar fracture toughness, Composite Structures 182 (2017) 153–163.

[44] X. Xu, M. R. Wisnom, X. Sun, S. R. Hallett, Experimental determination of through-thickness compression (ttc) enhancement factor for mode ii fracture energy, Composites Science and Technology 165 (2018) 66–73.

[45] M. Caminero, I. García-Moreno, G. Rodríguez, Experimental study of the influence of thickness and ply-stacking sequence on the compression after impact strength of carbon fibre reinforced epoxy laminates, Polymer Testing 66 (2018) 360–370.

[46] C. Soutis, P. Curtis, Prediction of the post-impact compressive strength of CFRP laminated composites, Composites Science and Technology 56 (6) (1996) 677–684.

[47] R. Talreja, N. Phan, Assessment of damage tolerance approaches for composite aircraft with focus on barely visible impact damage, Composite Structures 219 (2019) 1–7.

[48] N. Baker, R. Butler, C. B. York, Damage tolerance of fully orthotropic laminates in compression, Composites Science and Technology 72 (10) (2012) 1083–1089.

List of Figures

List of Tables

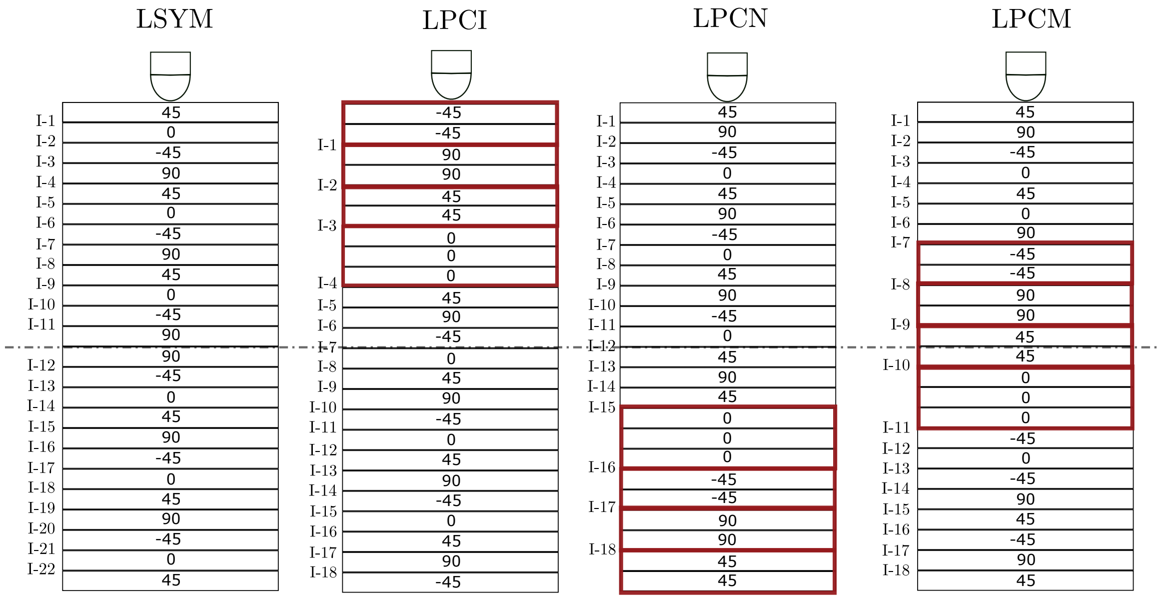

Figure 1: Illustration of all the laminates used for the study: LSYM, LPCI, LPCN and LPCM, where LPCN is obtained by flipping upside down LPCI. Note that T (top), B (bottom) and M (middle) refer to the location of the clustered block in the through-the-thickness direction of the laminate.

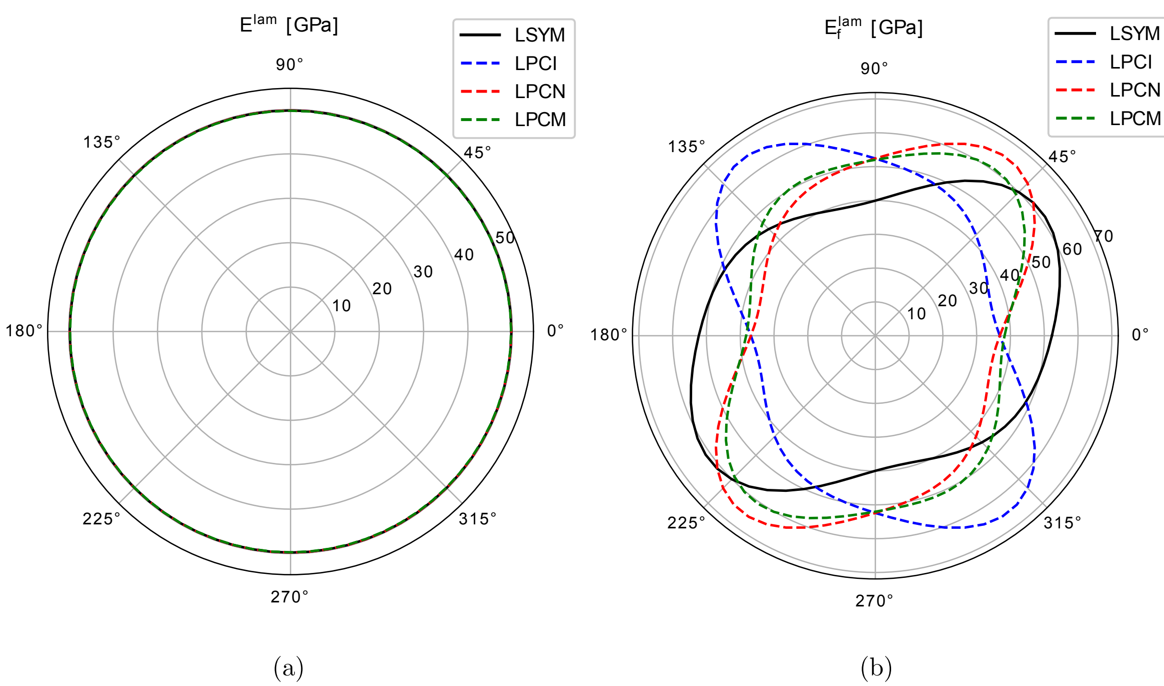

Figure 2: Polar plot representation of the (a) in-plane stiffnesses and (b) bending stiffness of all the laminates.

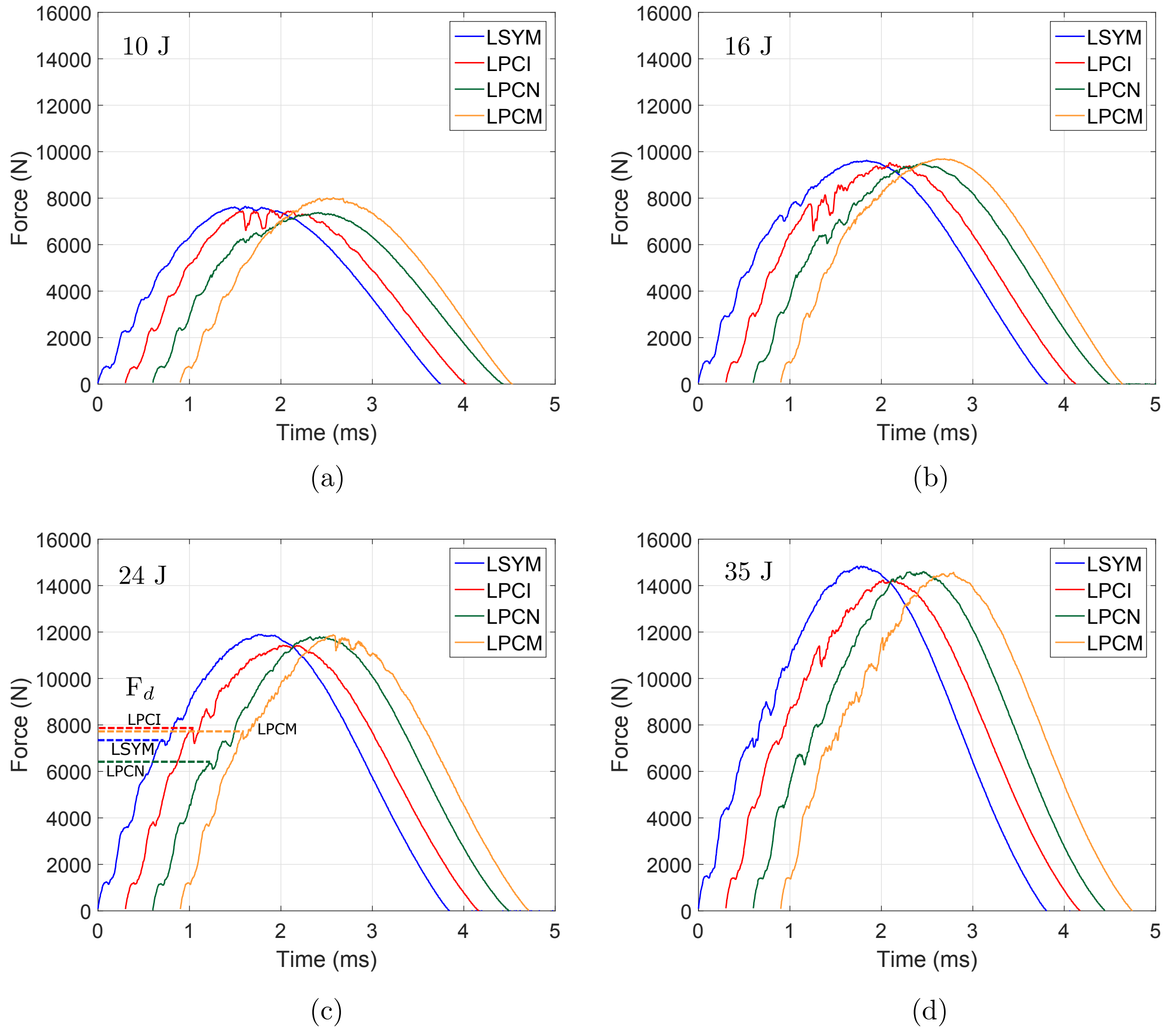

Figure 3: Impact force-time response curves of all laminates for all impact energies (Note that the responses of LPCI, LPCN and LPCM are offset by 0.3, 0.6 and 0.9 ms from LSYM, respectively, for proper comparison)

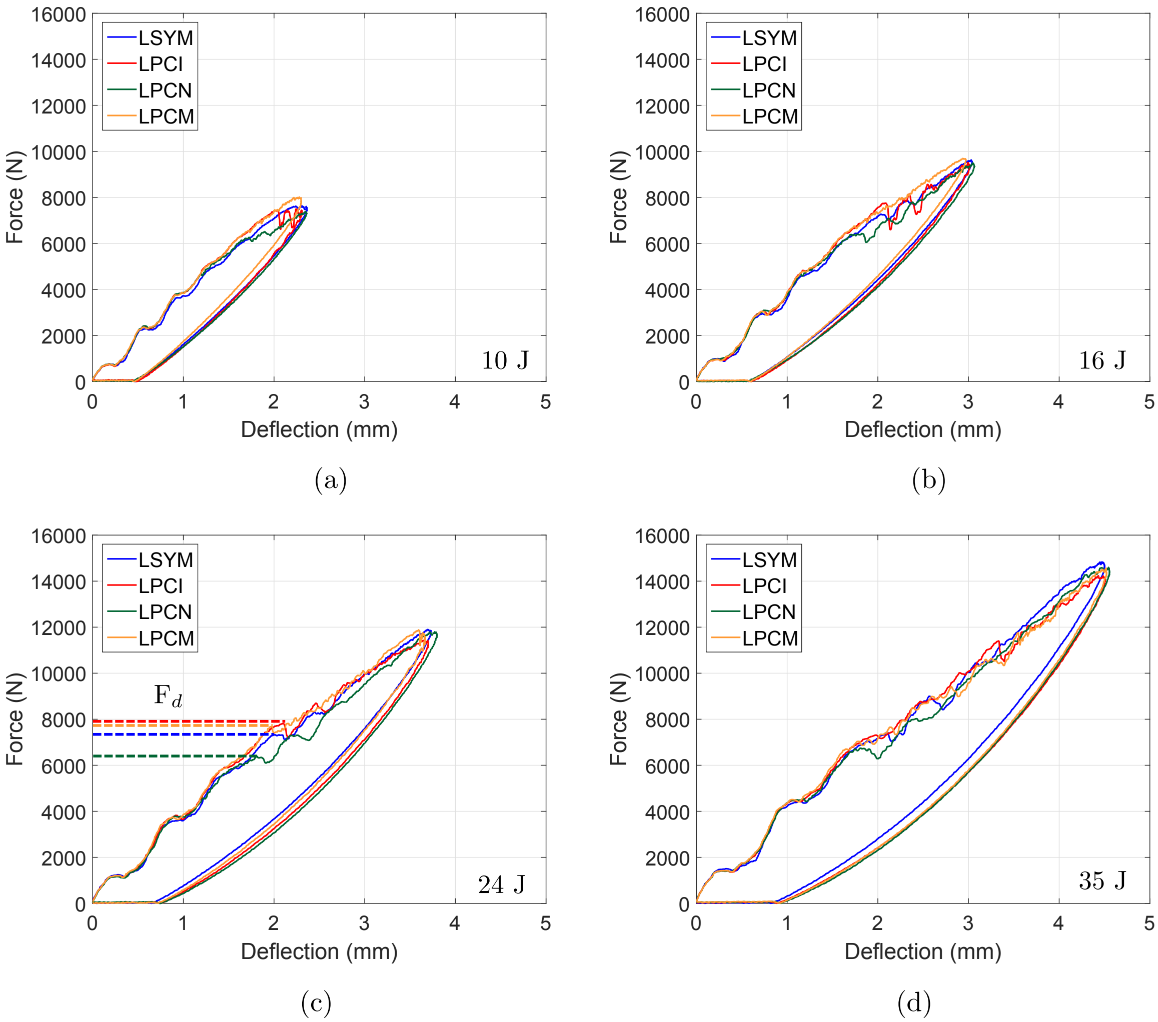

Figure 4: Impact force-deflection response curves of all laminates for all impact energies

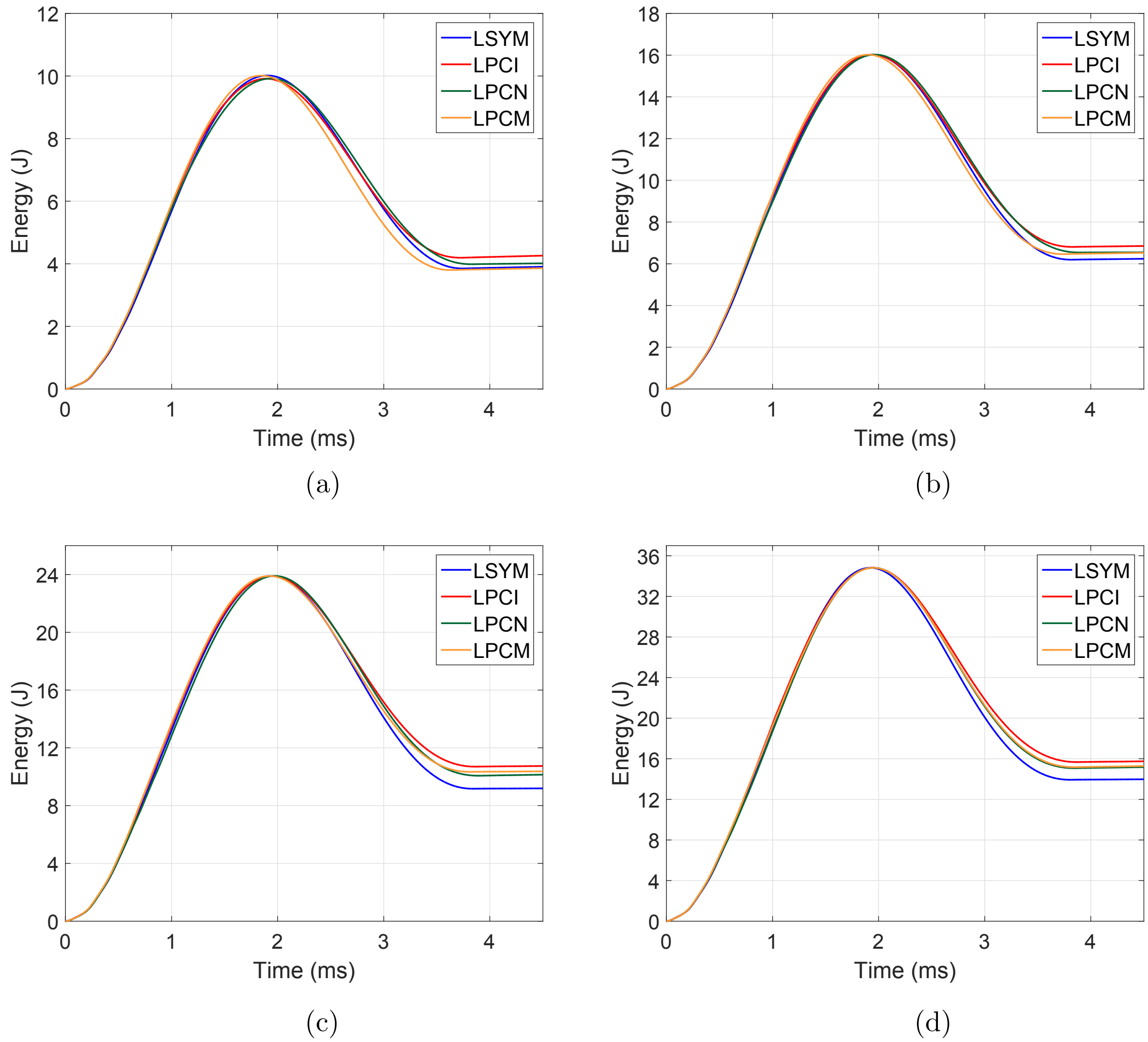

Figure 5: Impact energy-time response curves of all laminates for all impact energies

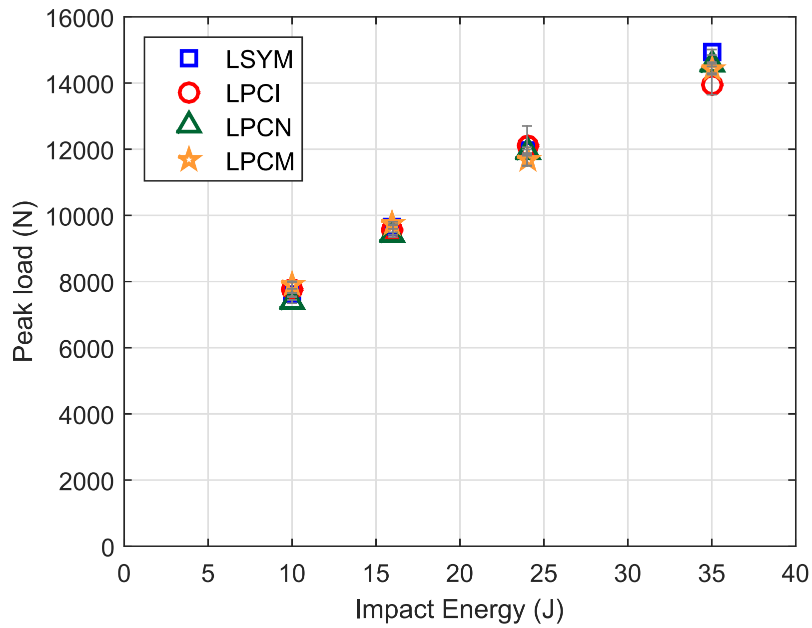

(a)

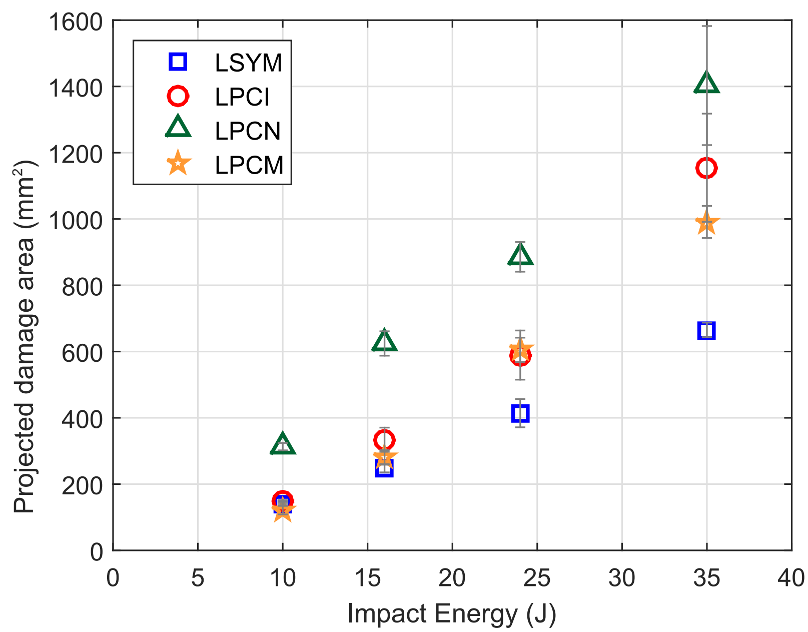

(b)

Figure 6: Impact damage resistance parameters (a) peak load and (b) projected damage area for all laminates for all impact energies

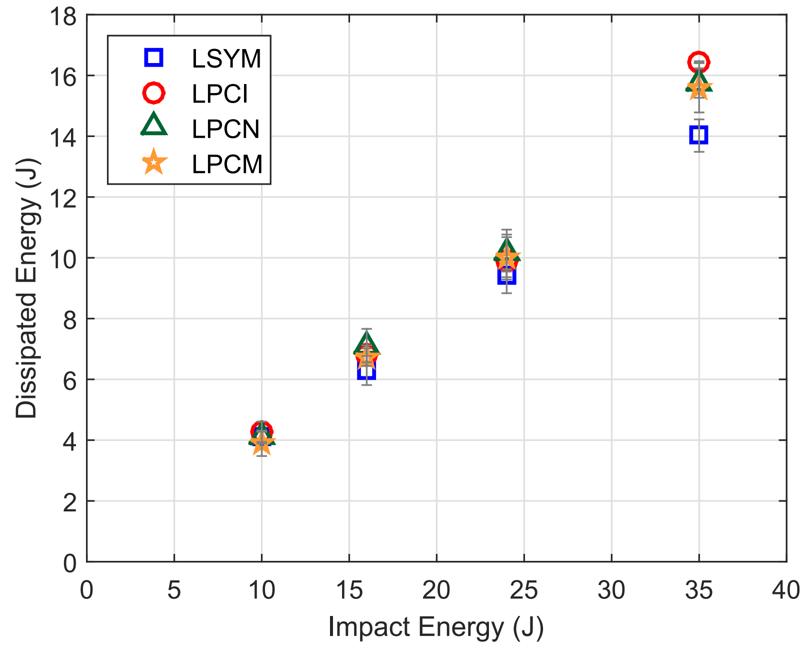

(a)

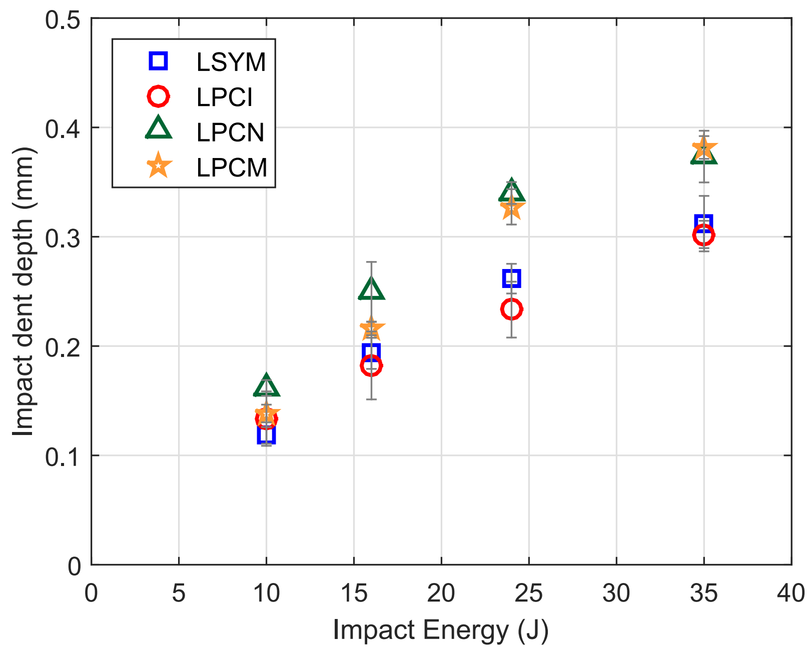

(b)

Figure 7: Impact damage resistance parameters (a) dissipated energy and (b) impact dent depth for all laminates for all impact energies

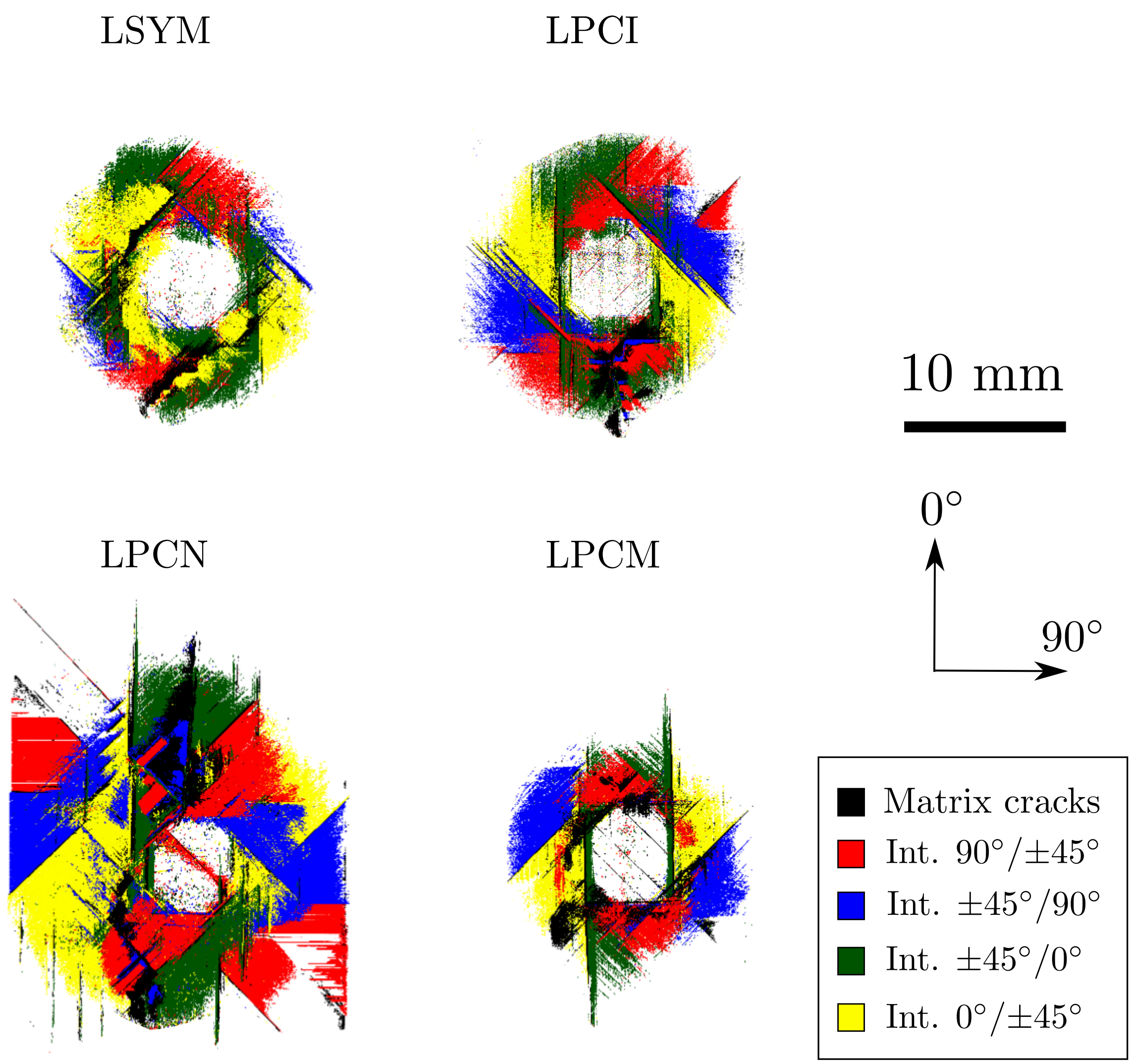

Figure 8: Projected damage footprint of all the laminates obtained from the post-processed μCT slices of the 10 J impact. Delaminations at different interfaces and matrix cracks are represented using colour codes as given in the legend and the represented field of view is 22 mm for all the laminates.

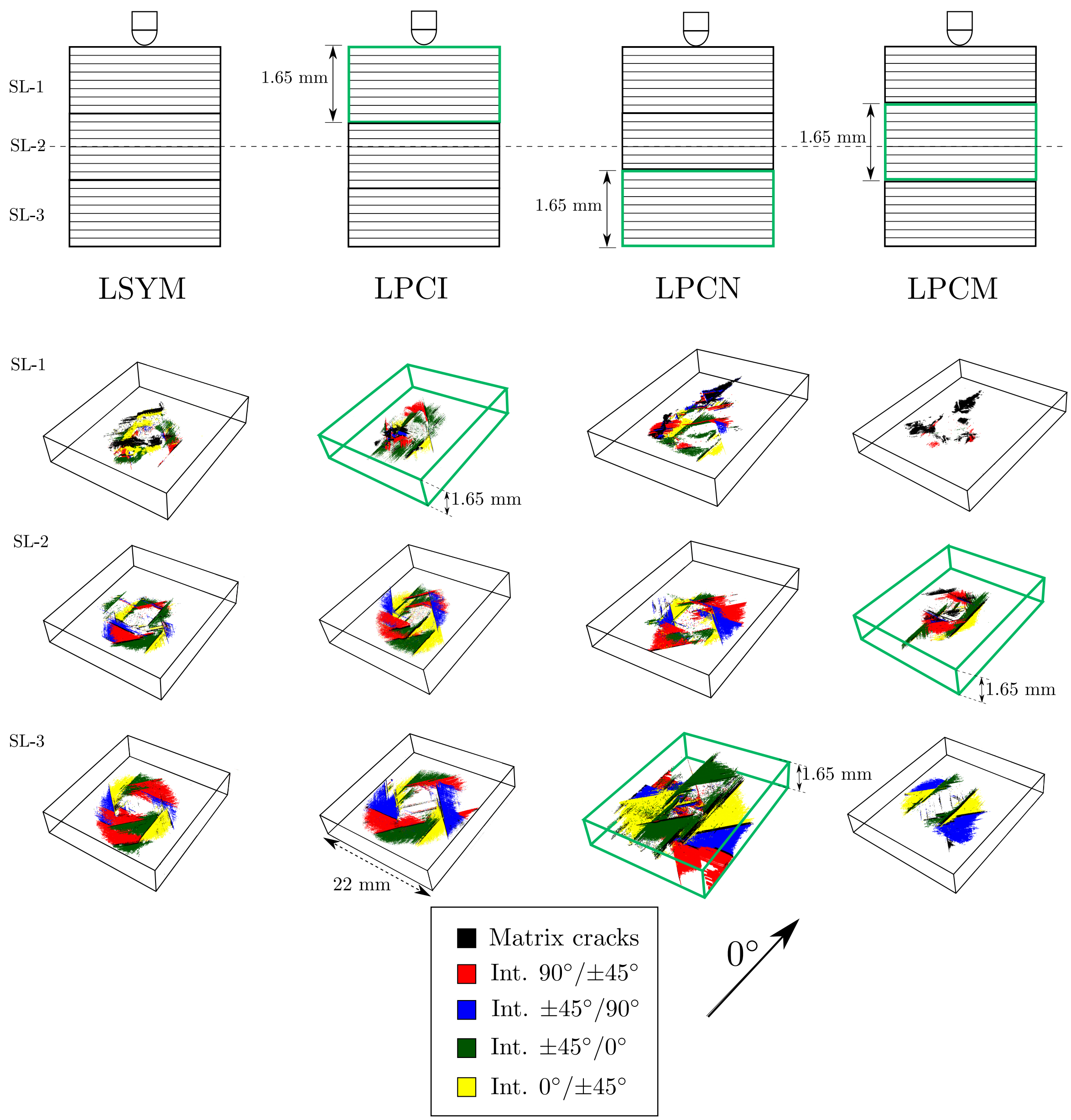

Figure 9: A 3D extruded illustration of the damage obtained from the post-processed μCT slices of the 10 J impact. Each laminate is divided into three sub-laminates and the sub-laminate containing the clustered plies of each unsymmetrical laminate is marked by a green box.

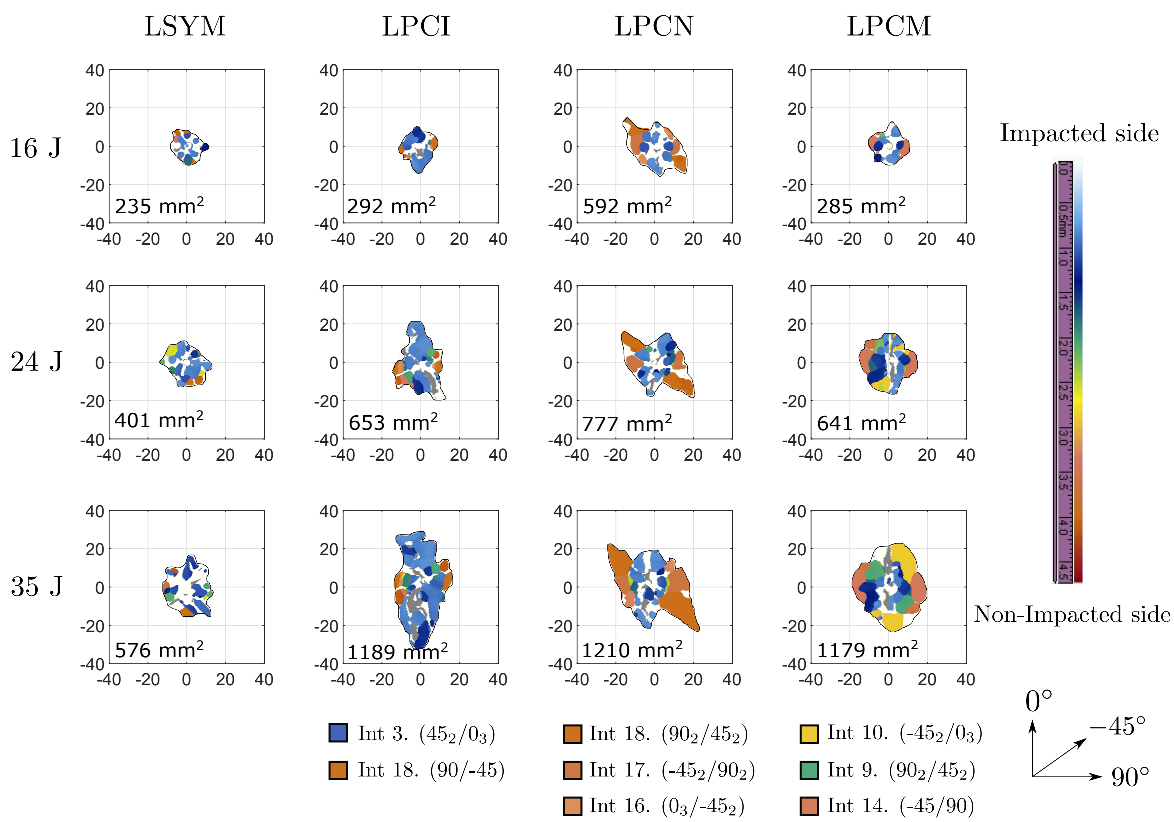

Figure 10: C-scan images of all four laminates inspected from the impacted side for the impact energies 16, 24 and 35 J. Projected delamination area is marked in the bottom left corner of each box and the field of view represented is 80 x 80 mm with the impact point as the centre.

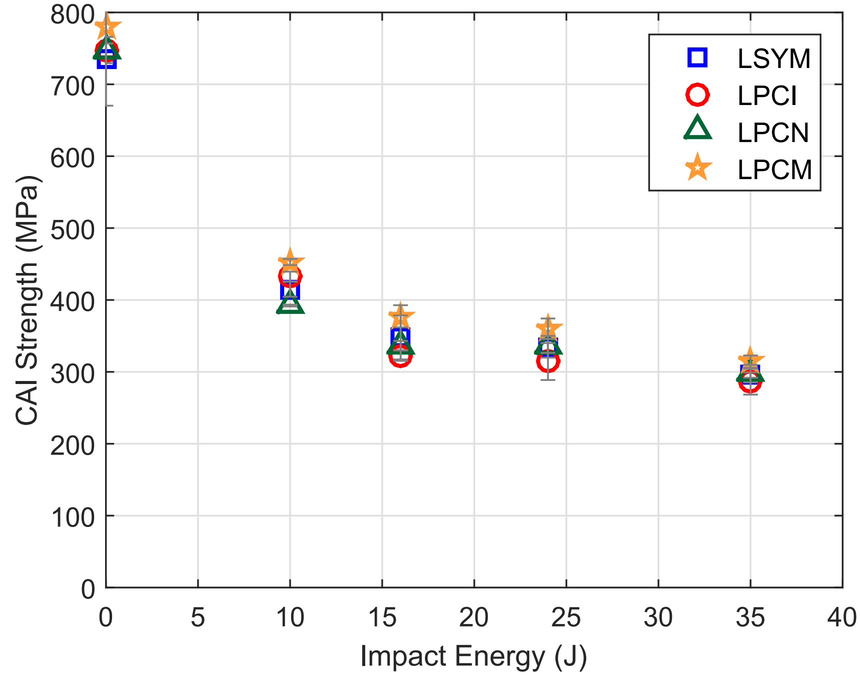

(a)

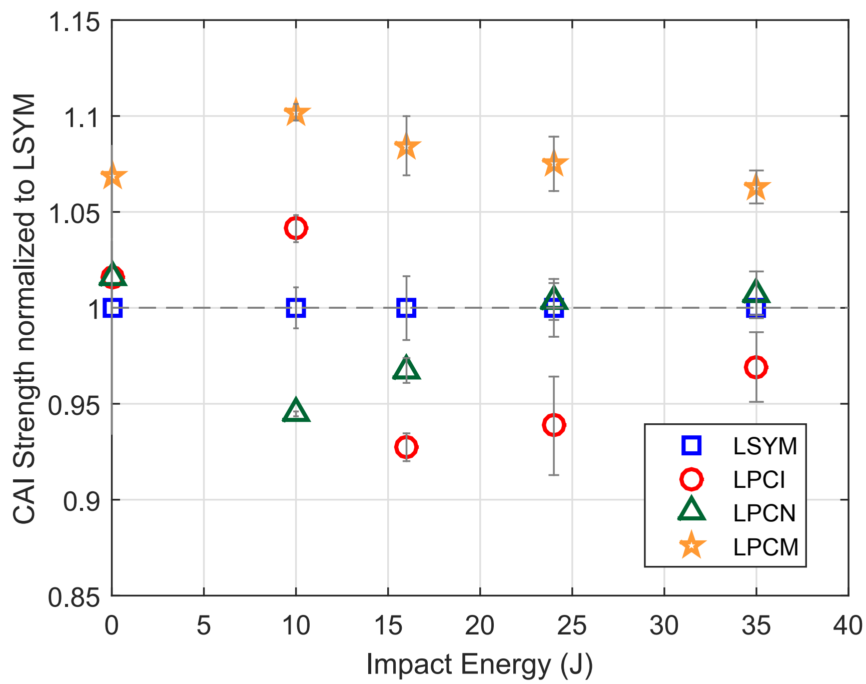

(b)

Figure 11: (a) Absolute and (b) Normalized (with respect to LSYM baseline) plain compression strengths and CAI strengths of all four laminates for all impact energies.

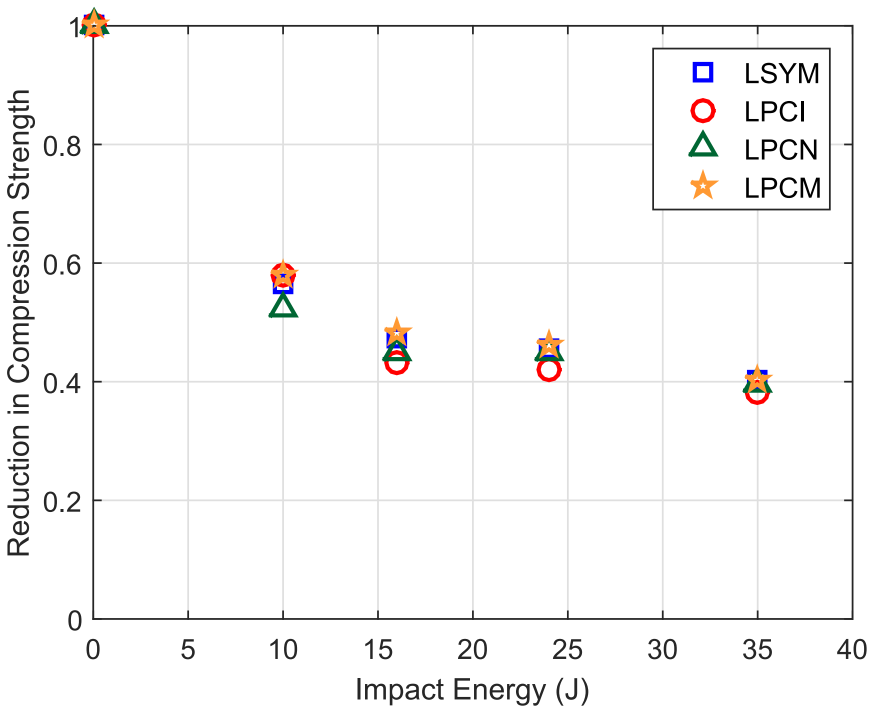

Figure 12: Normalized reduction in the compression strength due to the impact induced damage for all the impact energies.

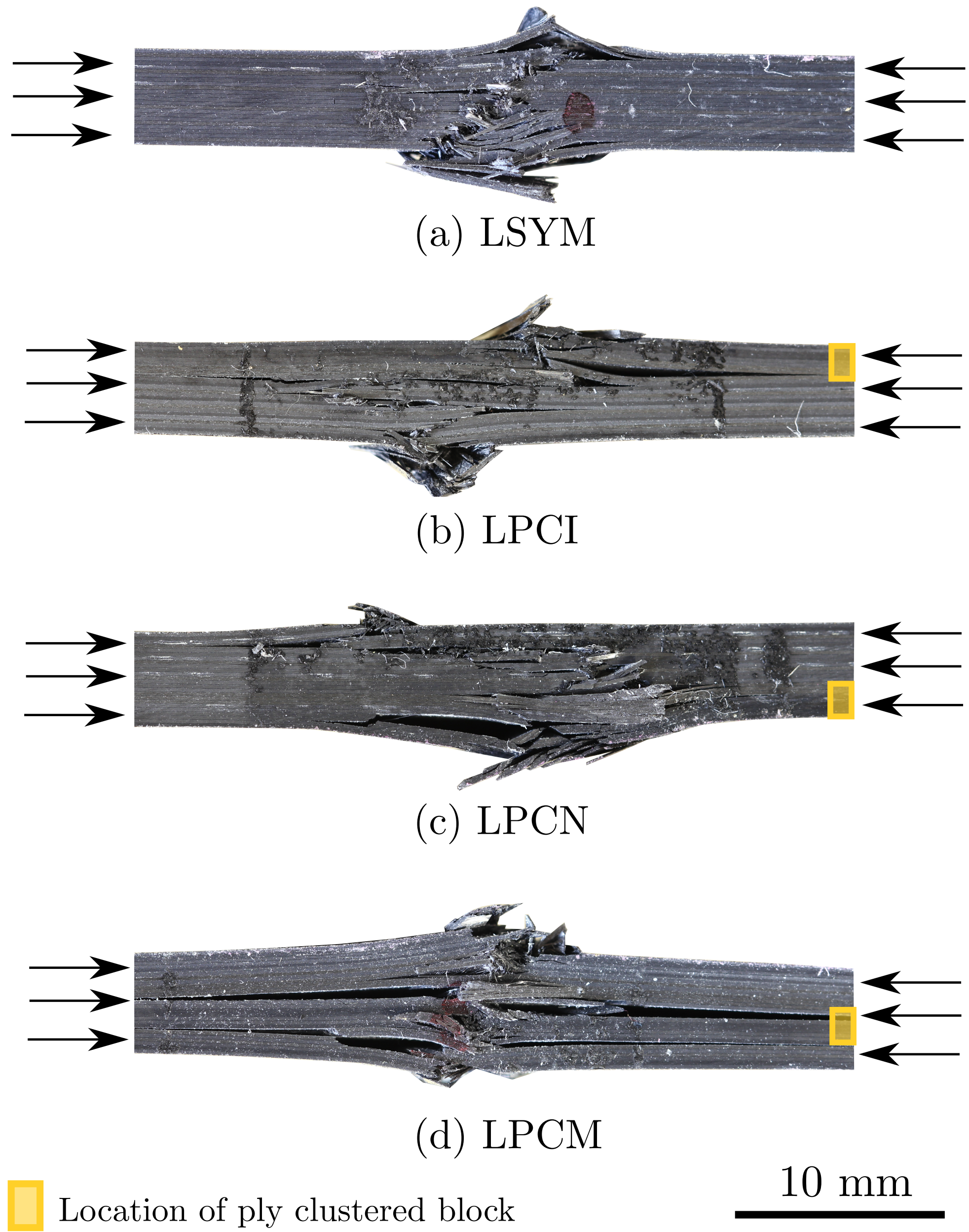

Figure 13: High resolution macro photos of the specimen edges showing the final CAI failure state of all four laminates (location of the clustered block is shown by the yellow box).

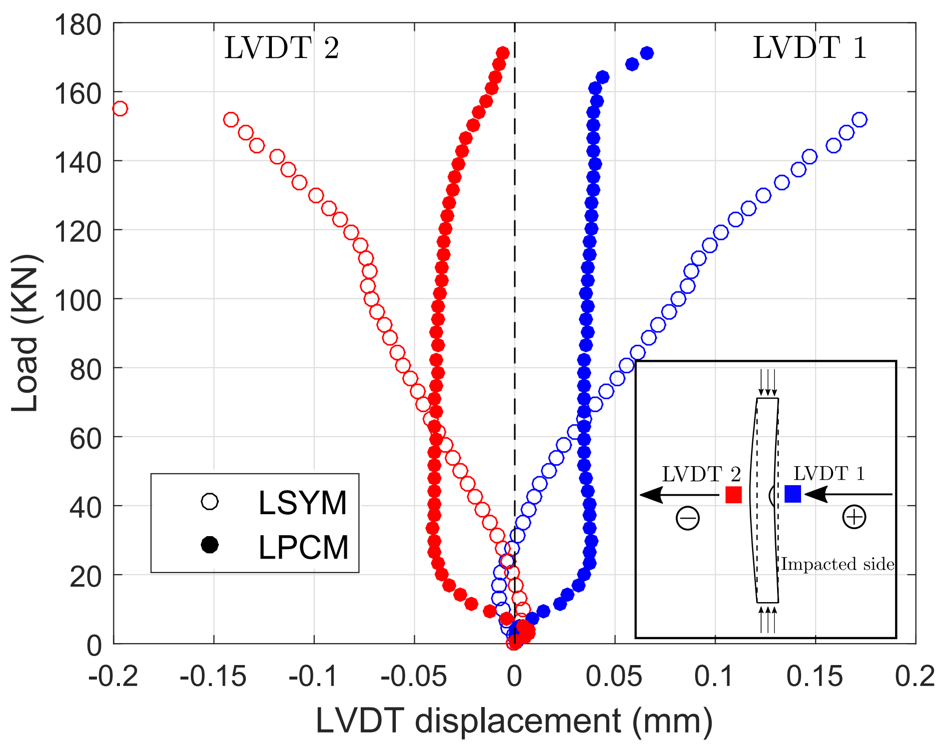

Figure 14: Out-of-plane displacements recorded by the LVDTs placed at the impacted and non-impacted face laminate centres during the CAI loading of a 16 J impact for LSYM and LPCM laminates (Note that blue indicates LVDT 1 placed at the impacted side and red indicates LVDT 2 placed at the non-impacted side. Outwards buckling (shown by the black arrows in the sub-figure) is indicated by positive values of LVDT 1 and negative values of LVDT 2).

Table 1: Laminates and their details

Laminate	Description	Stacking sequence (impacted side to non-impacted side)
LSYM	Symmetric baseline [27]	$[45/0/\text{-}45/90]_{3s}$
LPCI	Unsymmetric, Clustered block at the top	$[\text{-}45_2/90_2/45_2/0_3/45/90/\text{-}45/0/45/90/\text{-}45/0/45/90/\text{-}45/0/45/90/\text{-}45]$
LPCN	Unsymmetric, Clustered block at the bottom	$[45/90/\text{-}45/0/45/90/\text{-}45/0/45/90/\text{-}45/0/45/90/-45/0_3/\text{-}45_2/90_2/45_2]$
LPCM	Unsymmetric, Clustered block at the middle	$[45/90/\text{-}45/0/45/0/90/\text{-}45_2/90_2/45_2/0_3/\text{-}45/0/\text{-}45/90/45/\text{-}45/90/45]$